A Lagrangian Particle-based Formulation for Coupled Simulation of Fracture and Diffusion in Thin Membranes

Chengguizi Han[†]   Tao Xue[†]   Mridul Aanjaneya

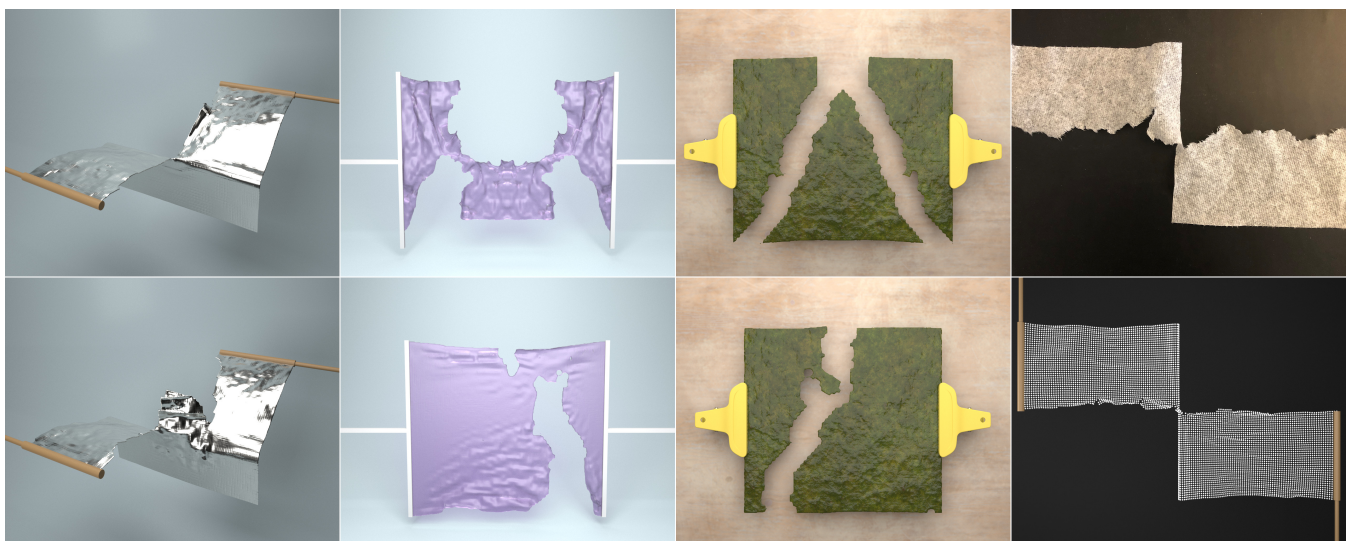Department of Computer Science, Rutgers University

Figure 1: *Our novel method allows for deformation, diffusion, and crack formation in thin membranes composed of different materials, such as foil (column 1), rubbery films (column 2), and seaweed flakes (column 3). (Top) Symmetric crack patterns without diffusion effects, and (bottom) asymmetric crack patterns due to diffusion of various quantities, such as temperature (in foil), acid solvent (in rubbery film), and moisture (in seaweed flakes). (Column 4) Our simulations of wet paper towel (bottom) qualitatively match real-world observations (top).*

Abstract

We propose a Lagrangian particle-based formulation for simulating deformation, fracture, and diffusion in thin membrane-like structures, such as aluminium foil, rubbery films, and seaweed flakes. We integrate our model with diffusion processes and derive a unified framework for simulating deformation-diffusion coupled phenomena, which is applied to provide realistic heterogeneity induced by the diffusion process to fracture patterns. To the best of our knowledge, our work is the first to simulate the complex fracture patterns of single-layered membranes in computer graphics and introduce heterogeneity induced by the diffusion process, which generates more geometrically rich fracture patterns. Our end-to-end 3D simulations show that our deformation-diffusion coupling framework captures detailed fracture growth patterns in thin membranes due to both in-plane and out-of-plane motions, producing realistically wrinkled slit edges, and heterogeneity introduced due to diffusion.

CCS Concepts
• **Computing methodologies** → *Computer graphics; Physical simulation;*

[†] Joint first authors

1. Introduction

Membrane-like deformable objects play an important role in computer graphics for representing clothes [LYO*10], paper [SRH17,
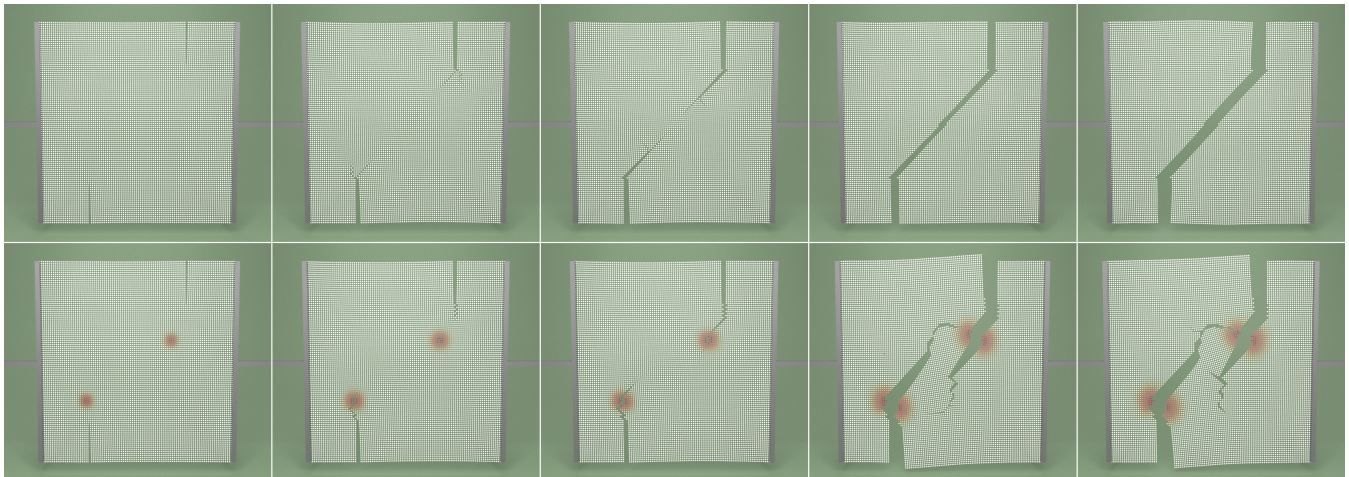
Figure 2: *Crack Path. We put two sources that emits diffusive matter in a pre-notched membrane. Our method captures symmetric cracks in the membrane without diffusion (top) and asymmetric crack propagation in the membrane with diffusion (bottom). The crack tip changes its path when it reaches close to the source spots. Diffusive quantities are visualized with colors from light red to dark red for increasing values.*

BDW13], biological tissues [DCL00], and shells [KMB*09]. Despite continuous deformations, such as stretching and bending, *fracture* is a complex material response for realistic animations and has drawn attention from numerous groups. Since a membrane-like object exhibits little deformation in the direction of its thickness, complaint thin membranes in the real world often have more complex fracture behavior, particularly when non-homogeneous material properties are considered. Examples of such materials include leather, skin, wet paper, plywood, and composite cloth.

The conventional approach for simulating general deformable objects, not only in computer graphics but also in engineering, relies heavily upon classical solid mechanics where the governing equations of motion are described by partial differential equations (PDEs). Such formulations suffer from inherent limitations when applied to problems involving material failure since the spatial derivatives do not exist on crack tips or crack surfaces, making the differential equations invalid on these singularities. Consequently, numerical discretization techniques such as the Finite Element Method (FEM) [ZTNZ77, GSH*04, LYO*10, SB12] and Material Point Method (MPM) [WFL*19, WCL*20], are not always satisfactory, either physically or mathematically, in part because of the need for supplemental relations that control the growth of cracks. Similar issues also arise in simulations of other PDEs that describe the evolution of physical fields, such as diffusion processes, in materials with discontinuities.

In contrast to PDE-based descriptions of the governing equations of motion, *integral* formulations [Cru77, Lad00] for deformable objects offer an attractive alternative that avoids the spatial singularities that arise due to the presence of discontinuities. Among them, *peridynamics* [Sil00, SL10] has been widely adopted in engineering, which is a *non-local* reformulation of PDE-based continuum mechanics. Unlike the classical theory, the state of a material point is influenced not only by material points located in its immediate vicinity, but also by those from over long distances. The governing equations of motion in peridynamics are spatial integral equations instead of PDEs. The peridynamics model has been recently

investigated in computer graphics [LBC*14, CZZ*18, LZC*19, HWW17] for simulating fracture in volumetric deformable objects.

The crack path in thin membranes is extremely sensitive in real-world materials. Previous studies [PNDJO14, BDW13] have simulated crack propagation in membrane-like materials via FEM and the crack paths were purely decided by the deformation field of the material, while the influence of multi-physics on crack paths has not been investigated in graphics. Diffusion, such as temperature change in foils, is one of the common causes that affects the crack paths in nature as it introduces extra diffusion-driven stress into material constitutive laws (see equations (18), (19), and (20)). Such diffusion-driven stress appears to be significant in thin membranes and triggers *heterogeneity* of dynamic responses exhibiting arbitrary fracture patterns in membranes (see Figure 2). In the present work, we propose a Lagrangian particle-based model to simulate fracture and diffusion processes in *thin membranes*. Instead of describing the governing equations of motion with PDEs [Gur82] and discretizing these PDEs, our formulation is an integral expression similar to peridynamics [HWW17, CZZ*18, LBC*14], such that it can readily handle simulations involving fractures without suffering from the issue of spatial singularities on crack tips. Our main contributions are as follows:

1. A Lagrangian particle-based model that directly provides integral formulations for coupled simulation of deformation-diffusion phenomena with fracture in membrane-like objects.
2. A novel criterion for automatically updating fracture growth.
3. End-to-end simulations of stretching, tearing, and heterogeneity induced by diffusion to highlight the versatility of our method.

2. Related Work

In this work, we only review prior work related to simulations for membrane-like structures since our focus is on thin structures. However, we note that there are numerous established models to simulate volumetric deformable objects with fracture, since it is a well-studied problem in both engineering and computer
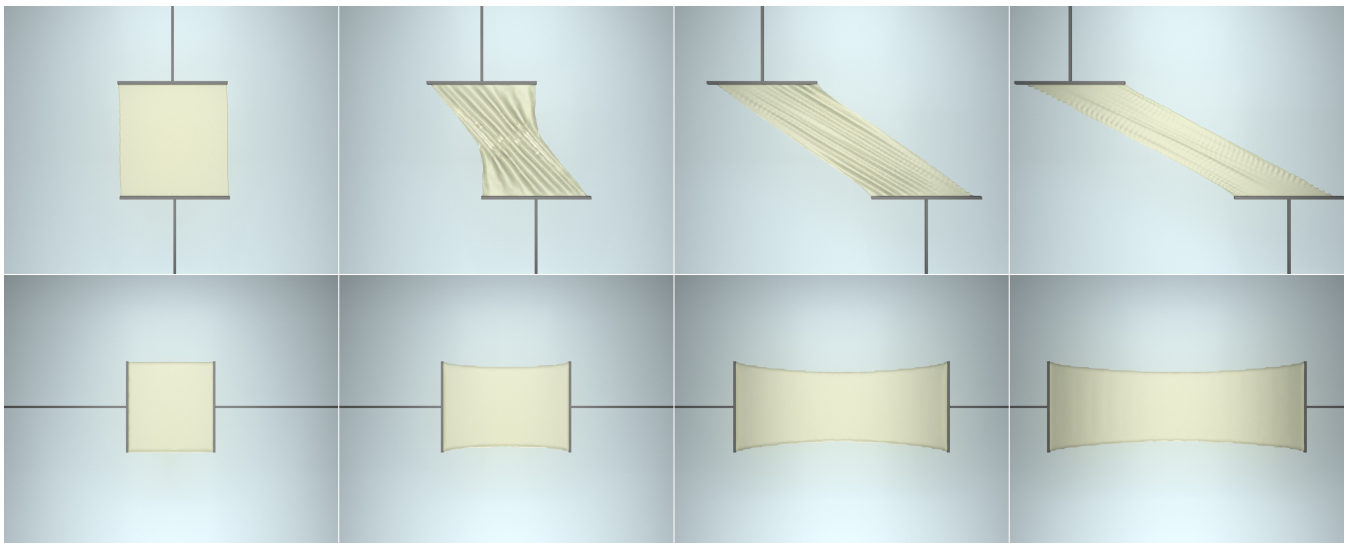
Figure 3: *Large deformation. Our model captures the large shearing (top) and stretching (bottom) deformation.*

graphics [MBF04, SDF07, HJST13, KBT17, WDG*19, WFL*19, WCL*20]. An early survey regarding deformable models in computer graphics was given in [NMK*06] which provides an easy entry point for researchers and developers who are new to this field.

2.1. Deformation of membrane structures

Physics-based simulations for membrane structures, such as paper, cloth, and foil, have a long history in computer graphics. The simple mass-spring system was largely used in early work [CK05, P*95, BFA02], where the governing equations were a nodal-discretized Newton's second law. Later, unlike mass-spring models, finite-strain theory from classical continuum mechanics [ZTTT00] was utilized to describe deformable bodies, in which the intuitive governing equations are a set of partial differential equations (PDEs). To discretize those PDEs, mesh-based discretization techniques, such as the Finite Element Method (FEM) [ZTNZ77, SB12] were used. Later, FEM simulations for thin shells [KMB*09] became a popular research topic in computer graphics. On the other hand, mesh-free methods, such as SPH [PGBT18] and position-based dynamics [MHHR07, MMC16] are also proposed to simulate systems with small thickness. Besides, the Material Point Method (MPM) [JGT17] was recently adopted to simulate cloth due to its convenience of merging the advantages of both particles and grids in the discretization.

In contrast to PDE-based simulations, a spatial integral formulation for continuum mechanics, named *Peridynamics*, was recently proposed in engineering [Sil00, SL10]. Since its essence is to use integration to compute the forces on a material particle, it can easily handle systems with fracture. This integral formulation for continuum mechanics has also been introduced in computer graphics for simulations of deformable objects with fracture. Current research [CZZ*18, LZC*19, HWW17] has so far focused on peridynamics formulations for *volumetirc* objects and produced persuasive effects. However, a peridynamics formulation for membrane structures, which is surface-based, as well as its coupling with diffusion, remains unclear in graphics.

2.2. Fracture animation

Early work on fracture simulations in computer graphics dates back to [TF88, NTB*91], which formulates a simple stretching limit as the criterion for fracture initiation and growth. FEM-based fracture simulations of both brittle objects [OH99] and ductile objects [OBH02] were developed by O'Brien and his collaborators. Later, a virtual node method [SDF07, MBF04] in the FEM framework was proposed to embed cracks in virtual elements to prevent stability issues. XFEM embedding [KMB*09, KBT17] can accurately resolve dynamics along the crack path, but imposes limits on the fracture geometry and can be costly for complicated fracture patterns. Instead of simulating fractures using meshes, researchers have also studied other representations, including particle systems [DCL00, Mül08, WDG*19], arbitrary polyhedra [WSG05, MKB*08, HJST13], and point clouds [PKA*05, SOG06]. Moreover, MPM-based fracture, such as CRAMP [Nai03, GN06], provides an additional approach to fracture simulations. Recently, a variational phase-field approach was integrated with MPM to animate isotropic [WFL*19] and heterogeneous fractures [WCL*20].

3. Overview of Lagrangian Formulation for PDE-based Coupling of Deformation and Diffusion

In this section, we provide an overview of the Lagrangian methodology and demonstrate how it can be used to derive the traditional PDE-based governing equations for coupling deformation and diffusion, such as those that arise in thermoelasticity [AD12, XZT19, XSH*20]. The resulting equations are formulated as *differential equations*, which assume sufficient smoothness conditions. In other words, any spatial discontinuity, such as fracture, violates the continuity condition and causes differential terms in space to become non-differentiable. This assumption also makes sense in either the weak-form discretization, such as FEM [ZTNZ77], or strong-form discretization, such as SPH [MST04], of the governing equations.
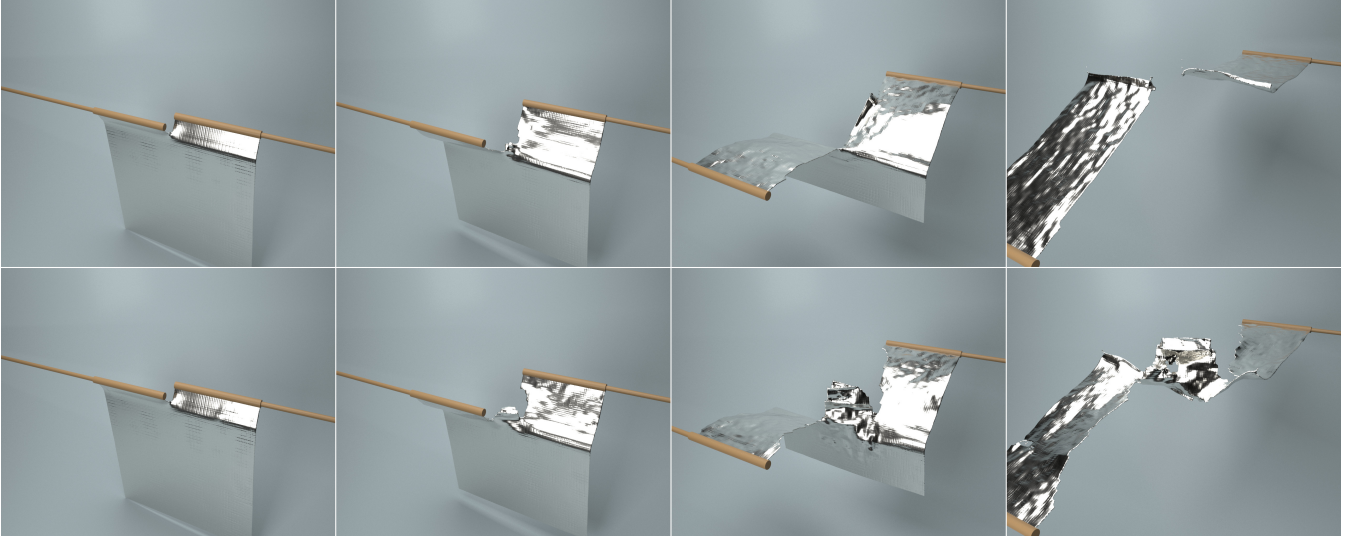
Figure 4: *Tearing foil. We tear an aluminum foil demonstrating that our method can simulate fractures by out-of-plane motions. We heat the sheet up by 100 heat spots randomly located on the sheet and observe the crack propagation under thermal stress. Our method captures a "clean" fracture pattern in the foil without any thermal stress (top), and heterogeneous fracture patterns with thermal stress (bottom).*

3.1. Deformation

The Lagrangian $\mathcal{L}$ for a deformable object is defined as:

$$\mathcal{L}(\mathbf{q}, \dot{\mathbf{q}}) = \mathcal{K}(\dot{\mathbf{q}}) - \mathcal{U}(\mathbf{q}), \tag{1}$$

where $\mathbf{q}$ is the generalized displacement, $\dot{\mathbf{q}}$ is the generalized velocity, $\mathcal{K}(\dot{\mathbf{q}})$ is the kinetic energy, and $\mathcal{U}(\mathbf{q})$ is the potential energy. Since we also consider the potential energy introduced due to diffusion processes, such as heat transfer [XZT19] or moisture change [XSH*20], a diffusive quantity θ is introduced to the potential energy $\mathcal{U}$. By omitting the energy due to external body forces and traction for the sake of simplicity, the kinetic and potential energies can be defined as:

$$\mathcal{K}(\dot{\mathbf{q}}) = \frac{1}{2} \int_{\mathcal{B}} \rho^0 \dot{\mathbf{q}}^T \dot{\mathbf{q}} dV, \quad \mathcal{U}(\mathbf{q}, \theta) = \int_{\mathcal{B}} \Psi(\mathbf{F}, \theta) dV, \tag{2}$$

where ρ^0 is the material density, $\Psi(\mathbf{F})$ is the Helmholtz free energy per unit mass in homogeneous materials, and $\mathbf{F}$ is the deformation gradient tensor. θ is the quantity being diffused, such as the temperature or moisture. Under the assumption that all the physical variables are sufficiently smooth, we can define a Lagrangian density function as follows:

$$\bar{\mathcal{L}}(\mathbf{q}, \dot{\mathbf{q}}, \mathbf{F}) = \frac{1}{2} \rho \dot{\mathbf{q}}^T \dot{\mathbf{q}} - \Psi(\mathbf{F}, \theta). \tag{3}$$

Based on the Lagrangian framework [ZTNZ77] and the *condition of continuity*, the governing equations of motion are as follows:

$$\frac{d}{dt}\left(\frac{\partial \bar{\mathcal{L}}}{\partial \dot{\mathbf{q}}}\right) - \frac{\partial \bar{\mathcal{L}}}{\partial \mathbf{q}} = \mathbf{0}, \tag{4}$$

where

$$\frac{d}{dt}\left(\frac{\partial \bar{\mathcal{L}}}{\partial \dot{\mathbf{q}}}\right) = \rho \ddot{\mathbf{q}}, \quad \frac{\partial \bar{\mathcal{L}}}{\partial \mathbf{q}} = \frac{\partial \Psi(\mathbf{F}, \theta)}{\partial \mathbf{F}} \frac{\partial \mathbf{F}}{\partial \mathbf{q}}. \tag{5}$$

Note that the term $\partial \Psi(\mathbf{F})/\partial \mathbf{F}$ represents a stress tensor that is determined by the material constitutive model, and the term $\partial \mathbf{F}/\partial \mathbf{q}$ can be further expressed in terms of a divergence operator. These two terms together define the internal force as the material deforms. In the present work, we utilize the total Lagrangian formulation, in which all the derivatives are evaluated with respect to the initial configuration at time t_0. By doing this, the PDE-based governing equations can be written as:

$$\rho^0 \ddot{\mathbf{q}} + \nabla^0 \cdot \mathbf{P} = \mathbf{b}, \tag{6}$$

where $\mathbf{P}$ and $\mathbf{b}$ represent the first Piola–Kirchhoff stress tensor and external body force density, respectively, and the differential operator $\nabla^0 \square = \partial \square / \partial \mathbf{q}_0$. The Piola–Kirchhoff stress includes stress due to deformation and diffusion, and is defined as follows:

$$\mathbf{P} = \mathbf{P}_D - (3\lambda + 2\mu)\alpha \mathbf{I}\theta, \tag{7}$$

where $\mathbf{P}_D$ represents the stress due to deformation. Depending on different constitutive models, one can get different concrete expressions for $\mathbf{P}_D$, λ and μ are Lamé parameters, and α is the coefficient of linear diffusion expansion in the material.

3.2. Diffusion

We consider the Fourier model for diffusion [BILD11]. Thus, the governing equations are described as:

$$\rho C \frac{\partial \theta}{\partial t} = \nabla \cdot (k\nabla\theta) + S, \tag{8}$$

where θ is the quantity being diffused, S is the diffusive source/sink, ρ is the material density, C is the diffusive capacity, and k is the coefficient of diffusion. Our method can also be integrated with non-Fourier diffusion, such as the *C-F diffusion model* [XSH*20]. However, we do not pursue this direction in our present work.

4. Lagrangian Particle-based Framework for Thin Structures

Inspired by [SB05, HHB11], we now derive a Lagrangian particle-based framework for single-layered membrane-like structures. In our formulation, physical quantities are defined on particles rather
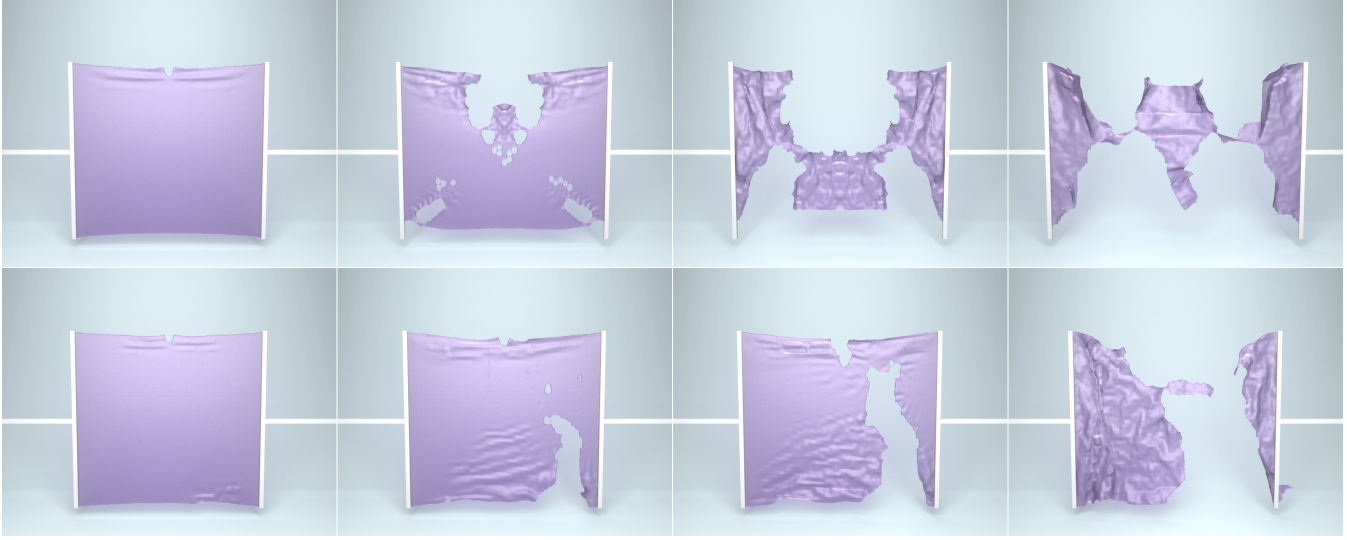
Figure 5: *Stretching rubbery film. We stretch a thin rubbery film with a small slit on the top edge (top). We randomly spray acid solvent on the film that diffuses and causes biodegradability, subsequently leading to arbitrary fracture patterns (bottom). Our method captures vivid wrinkles along the edges and produces rich dynamic response of the film rebounding after it has been completely damaged.*

than grids and the damage is handled by blocking the influence from neighboring particles instead of eliminating material particles. Different material models, such as linear and non-linear elasticity, or elastoplasticity, are supported in our framework. The resulting formulation is integral-based in space and does not require the condition of continuity, in contrast to alternative formulations that are PDE-based. Figure 6 gives a data flow of our Lagrangian Particle-based framework for thin structures.

4.1. Membrane Lagrangian

Since a membrane-like structure is very thin and offers little resistance to bending, we consider the Lagrangian in equation (4) to be defined on an *area*, unlike its volumetric counterpart. We define a position vector as $\mathbf{q}_i$ and diffusive quantity at $\mathbf{q}_i$ as θ_i. The Lagrangian at $\mathbf{q}_i$ in a neighborhood Ω_i is formulated as follows:

$$\mathcal{L}_i = \int_{j \in \Omega_i} \left[\frac{1}{2} \rho_j^0 (\dot{\mathbf{q}}_j)^T \dot{\mathbf{q}}_j - \Psi(\mathbf{F}_j, \theta_j) \right] dA, \qquad (9)$$

where $\mathbf{q}_j$ represents any arbitrary position located in Ω_i. When $\Omega_i \to 0$, under the condition of continuity, a Lagrangian density function such as equation (3), can be defined to replace equation (9) for further derivations, and leads to a PDE-based governing equation (see equation (6)). However, since our goal is to simulate a fracturing body, we use equation (9) to derive our formulation. We assume that there is a *micro-spring* between any two neighboring points that accounts for both deformation and diffusion. The stretch in this micro-spring can be defined as:

$$s_{ij} = \frac{\|\mathbf{r}_{ij}\|}{\|\mathbf{r}_{ij}^0\|}, \qquad (10)$$

where $\mathbf{r}_{ij} = \mathbf{q}_j - \mathbf{q}_i$ in the current configuration, and $\mathbf{r}_{ij}^0 = \mathbf{q}_j^0 - \mathbf{q}_i^0$ in the initial (i.e., resting) configuration at time t^0. These two distance vectors satisfy the relation:

$$\mathbf{r}_{ij} = \mathbf{F}_i \mathbf{r}_{ij}^0, \qquad (11)$$

where $\mathbf{F}_i$ denotes the deformation gradient at $\mathbf{q}_i$. In this way, this stretch value s_{ij} can be treated as the deformation ratio, and assumed to play the same role as the deformation gradient tensor in a volumetric system. As a natural extension, a scalar strain can also be defined as $\eta_{ij} = s_{ij} - 1$. Based on equation (4), η_{ij} is produced by a competition between the deformation and diffusion energies, and the free energy Ψ_{ij} for different materials [XZT19, LS67] can be defined as:

1. Linear elasticity

$$\Psi_{ij} = \frac{1}{2} c \eta_{ij}^2 - (3\lambda + 2\mu)\alpha\theta_j \eta_{ij}, \qquad (12)$$

where c is a positive constant describing the stiffness of the spring (see equation (24) for the specific expression for c).

2. Non-linear elasticity
We use the following non-linear elasticity (power law) model [Tre44] to describe rubbery membranes:

$$\Psi_{ij} = c \left(s_{ij}^2 + \frac{1}{s_{ij}^2} \right) + c^\star s_{ij}^n - (3\lambda + 2\mu)\alpha\theta_j \eta_{ij}, \qquad (13)$$

where $c^\star \leq 0$ and $n > 1$ are user-defined constants.

3. Elastoplasticity
To describe elastoplasticity, we assume that the deformation is elastic and reversible if $\eta < \eta_0$. However, when $\eta \geq \eta_0$, the deformation becomes irreversible and plastic. In this case, the Lagrangian is given as follows:

$$\Psi_{ij} = \begin{cases} \frac{1}{2} c \eta_{ij}^2 - (3\lambda + 2\mu)\alpha\theta_j \eta_{ij}, & \eta_{ij} < \eta_0 \\ -\frac{c}{\beta}(\eta_{ij}^0)^2 e^{\left(-\beta \frac{\eta_{ij} - \eta_0}{\eta_0}\right)} - (3\lambda + 2\mu)\alpha\theta_j \eta_{ij}, & \eta_{ij} \geq \eta_0 \end{cases} \qquad (14)$$

where β is a user-defined parameter.

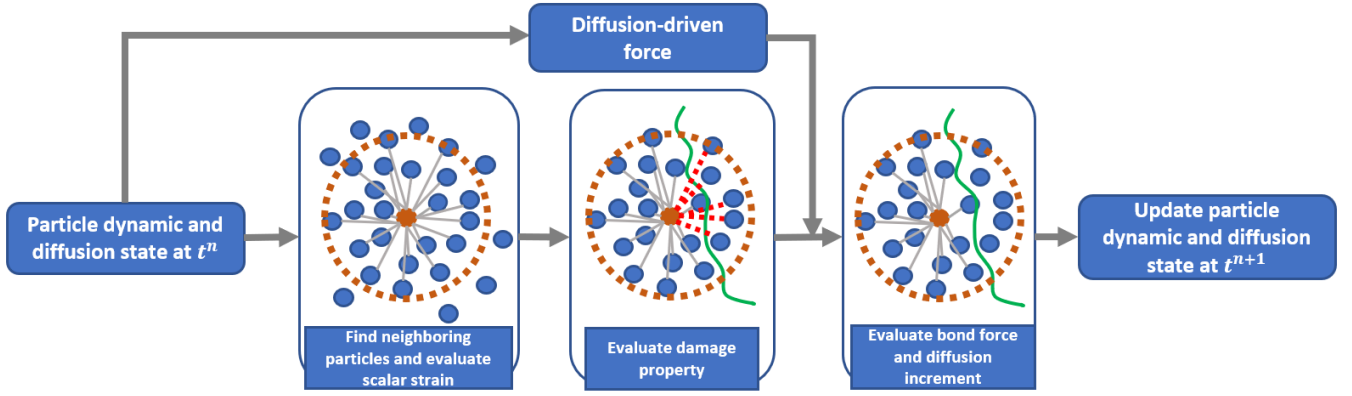To validate the above derivation, we briefly demonstrate that our 2D

Figure 6: *Overview of our proposed method. For simplicity, the orange circle is the influence range of its centered particle (also colored in orange), the grey lines are the virtual micro-bonds linking the centered particle and its neighboring particles, the green solid line is the crack path across the material, and the red dotted lines are the connected bonds that are cut by the crack surface. We remove these broken bonds when evaluating the dynamic and diffusion responses of all particles in our integral formulation, and update the particle states for time t^{n+1}.*

'micro-edge' free energy model given in equations (12)–(14) coincides with a reasonable classical elastic material in Appendix A. More detailed information can be found in [Sil00, HHB11].

4.2. Integral-based Equation of Motion

Next, we derive the integral-based equation of motion at position i via the Lagrangian in equation (9). Substituting the expression for $\mathcal{L}_i$ in equation (9) into equations (4) and (5) gives:

1. Kinetic term:

$$\frac{d}{dt}\left(\frac{\partial \mathcal{L}_i}{\partial \dot{\mathbf{q}}_i}\right) = \int_{j\in\Omega_i}\rho_j^0\ddot{\mathbf{q}}_j dA = \int_{j\in\Omega_i}\rho_j^0 dA\ddot{\mathbf{q}}_i = m_i^0\ddot{\mathbf{q}}_i, \quad (15)$$

where m_i^0 is the mass at position i.

2. Deformation term:

$$\frac{\partial \mathcal{L}_i}{\partial \mathbf{q}_i} = \int_{j\in\Omega_i}\frac{\partial\Psi(\mathbf{F}_j,\theta_j)}{\partial \mathbf{q}_i}dA = \int_{j\in\Omega_i}\frac{\partial\Psi(\mathbf{F}_j,\theta_j)}{\partial\eta_{ij}}\frac{\partial\eta_{ij}}{\partial \mathbf{q}_i}dA, \quad (16)$$

where $\partial\Psi(\mathbf{F}_j,\theta_j)/\partial\eta_{ij}$ is a scalar value representing the magnitude of the force between neighboring points i and j. We define f_{ij} as $\partial\Psi(\mathbf{F}_j,\theta_j)/\partial\eta_{ij}$, and equation (16) is rewritten as follows:

$$\frac{\partial \mathcal{L}_i}{\partial \mathbf{q}_i} = \int_{j\in\Omega_i}f_{ij}\frac{\partial\eta_{ij}}{\partial \mathbf{q}_i}dA = \int_{j\in\Omega_i}f_{ij}\frac{\mathbf{n}_{ij}^0}{\|\mathbf{r}_{ij}^0\|}dA, \quad (17)$$

where $\mathbf{n}_{ij}^0 = \mathbf{r}_{ij}^0/\|\mathbf{r}_{ij}^0\|$.

Substituting equations (12), (13), and (14) into equation (17) yields the following expressions for f_{ij} for different materials:

1. Linear elasticity

$$f_{ij} = c\eta_{ij} - (3\lambda + 2\mu)\alpha\theta_j \quad (18)$$

2. Non-linear elasticity

$$f_{ij} = 2c\left(s_{ij} - \frac{1}{s_{ij}^3}\right) + c^\star n s_{ij}^{n-1} - (3\lambda + 2\mu)\alpha\theta_j \quad (19)$$

3. Elastoplasticity

$$f_{ij} = \begin{cases} c\eta_{ij} - (3\lambda + 2\mu)\alpha\theta_j & \eta_{ij} < \eta_0 \\ c\eta_{ij}^0 e^{\left(-\beta\frac{\eta_{ij}-\eta_0}{\eta_0}\right)} - (3\lambda + 2\mu)\alpha\theta_j & \eta_{ij} \geq \eta_0 \end{cases} \quad (20)$$

Eventually, we have the integral-based equation of motion at position $\mathbf{q}_i$ as follows:

$$m_i\ddot{\mathbf{q}}_i = \int_{j\in\Omega_i}f_{ij}\frac{\mathbf{n}_{ij}^0}{\|\mathbf{r}_{ij}^0\|}dA + \mathbf{f}_i^{ext}, \quad (21)$$

where $\mathbf{f}_i^{ext}$ is external force at position i. As shown above, to derive equation (21), the condition of continuity is not required. We use *particles* to discretize equation (21) and introduce a weight function as follows:

$$m_i\ddot{\mathbf{q}}_i = \sum_j f_{ij}\frac{\mathbf{n}_{ij}^0}{\|\mathbf{r}_{ij}^0\|}W_{ij}^0 A_j^0 + \mathbf{f}_i^{ext}, \quad (22)$$

where A_j^0 is the area of particle j, W_{ij}^0 denotes the weight of particle j with respect to particle i in the initial configuration and is defined as:

$$W_{ij}^0 = \begin{cases} 1 - \frac{\|\mathbf{r}_{ij}^0\|}{R}, & \|\mathbf{r}_{ij}^0\| \leq R \\ 0, & \|\mathbf{r}_{ij}^0\| \geq R \end{cases} \quad (23)$$

where R is the cutoff radius and different values of R affect the stiffness of the micro-spring. In the present work, we use the stiffness coefficient c defined in [LBC*14] as:

$$c = \frac{18K}{\pi R^4}, \quad (24)$$

where K is the bulk modulus of the material.

4.3. Discrete Equation for Diffusion

To handle fractures, we use the following peridynamic model for heat transfer proposed in [BD10]:

$$\rho_i^0 C_i^0 A_i^0 \dot{\theta}_i = \sum_j k\left(\frac{\theta_j - \theta_i}{\|\mathbf{r}_{ij}^0\|^2} + S_i\right)W_{ij}^0 A_j^0. \quad (25)$$
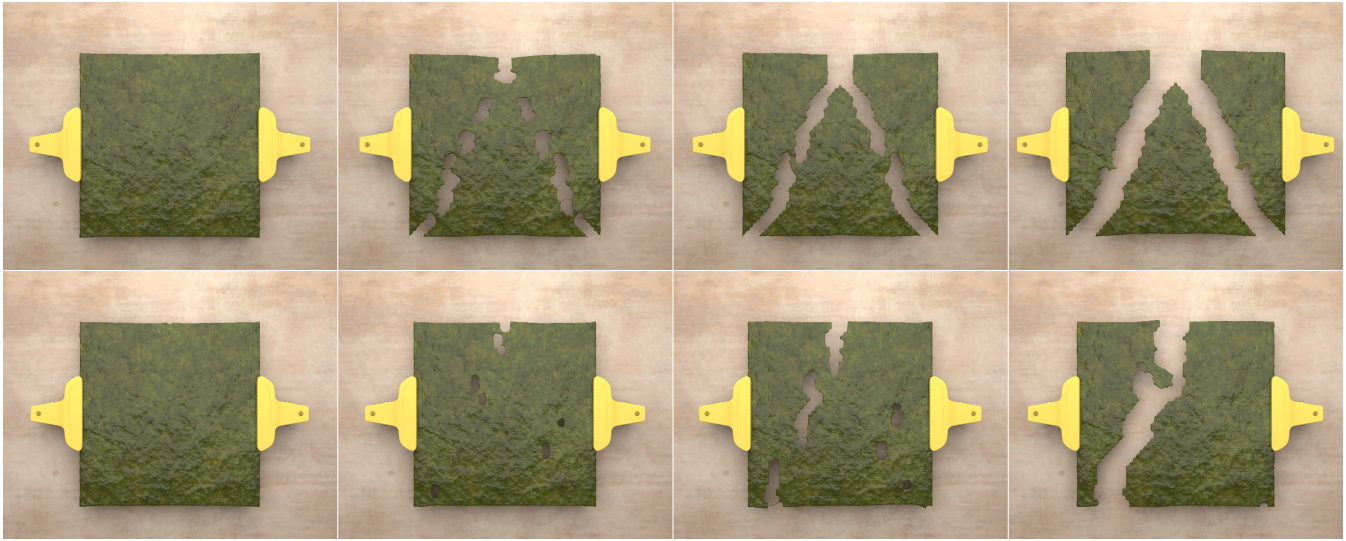
Figure 7: *Crispy and damp seaweed flake. Our method captures symmetric crack patterns in a dry seaweed flake when pulled apart along the side edges (top) and vividly asymmetric crack branches in a damp seaweed flake (bottom) under the additional effects of moisture diffusion.*

4.4. Temporal Discretization

Although implicit schemes have been acknowledged to be more efficient than explicit schemes and allow for larger time steps in the simulations, the time step Δt is required to be small to accurately capture fractures (which are high-speed events). Thus, we use forward Euler time integration in the present work, and update $\mathbf{q}_i$, $\dot{\mathbf{q}}_i$, and θ_i at time t^{n+1} as follows:

$$
\theta_i^{n+1} = \theta_i^n + \frac{\Delta t}{\rho_i^0 C_i^0 A_i^0} \left[\sum_j \left(k \frac{\theta_j^n - \theta_i^n}{\|\mathbf{r}_{ij}^0\|^2} + S_i^n \right) W_{ij}^0 A_j^0 \right]
$$

$$
\dot{\mathbf{q}}_i^{n+1} = \dot{\mathbf{q}}_i^n + \frac{\Delta t}{m_i} \left(\sum_j f_{ij}^n \frac{\mathbf{n}_{ij}^0}{\|\mathbf{r}_{ij}^0\|} W_{ij}^0 A_j^0 + \mathbf{f}_i^{ext} \right)
$$

$$
\mathbf{q}_i^{n+1} = \mathbf{q}_i^n + \Delta t \dot{\mathbf{q}}_i^{n+1}
$$

(26)

where the superscript n denotes variables at time t^n.

5. Fracture

Similar to peridynamics, the treatment of discontinuities is trivial due to the integral-based nature of our method. We model material damage by permanently breaking the micro-spring for deformation and diffusion. For elastoplastic materials, a simple critical stretch is generally used as the fracture criterion in peridynamics, which conforms to the physically plausible energy release rate, has been validated before [SA05], and was also utilized in computer graphics [HWW17,LBC*14]. In the present work, to merge both elasticity and plasticity, we define a parameter γ_{ij} featuring the damage of micro-spring $i \leftrightarrow j$ as follows:

$$
\gamma_{ij} = \begin{cases} 1, & \eta_{ij} \leq \eta_0 \\ e^{-\beta \frac{\eta - \eta_0}{\eta_0}}, & \eta_{ij} > \eta_0 \\ 0, & \eta_{ij} > \eta_c \end{cases}
$$

(27)

where η_0 denotes the elastic deformation limit and $\eta_c = \sqrt{4\pi G_f/9ER}$ denotes the fracture criterion, G_f, E, and R are the

material fracture energy, material Young's modulus, and cutoff radius, respectively. For elastic materials in equations (18) and (19) and the diffusion process in equation (25), γ_{ij} degenerates to:

$$
\gamma_{ij}^{\star} = \begin{cases} 1, & \eta_{ij} \leq \eta_c \\ 0, & \eta_{ij} > \eta_c \end{cases}
$$

(28)

Finally, the update equations considering fracture are given as follows:

$$
\theta_i^{n+1} = \theta_i^n + \frac{\Delta t}{\rho_i^0 C_i^0 A_i^0} \left[\sum_j \left(k \frac{\theta_j^n - \theta_i^n}{\|\mathbf{r}_{ij}^0\|^2} + S_i^n \right) (\gamma_{ij}^{\star})^n W_{ij}^0 A_j^0 \right],
$$

$$
\dot{\mathbf{q}}_i^{n+1} = \dot{\mathbf{q}}_i^n + \frac{\Delta t}{m_i} \left(\sum_j f_{ij}^n \frac{\mathbf{n}_{ij}^0}{\|\mathbf{r}_{ij}^0\|} \gamma_{ij}^n W_{ij}^0 A_j^0 + \mathbf{f}_i^{ext} \right).
$$

6. Results

We now present the results produced with our method in this section. All our membranes are discretized by a single layer of uniformly distributed particles, and the cutoff radius for the weight function in equation (23) is taken as $1.5\times$ the particle distance. All our examples were run on a 1.80 GHz, Intel(R) Core(TM) i7-8565K CPU with 8GB RAM. Table 1 summarizes the specific timings and the parameters used for all our examples.

6.1. Numerical Validation

We first simulate large shearing and stretching deformations in a thin sheet (without fracture) with a dimension of 2×2. As shown in Figure 3, our method produces realistic large deformation of the thin sheet and captures parallel folds in the shearing case (see Figure 3(top)). These folds occur because the membrane is free along the normal direction and therefore, tends to develop strains parallel to the shearing stress. It is worth noting that SPH methods, as well as other discretization techniques such as FEM, MPM and the like, provide the numerical approaches to approximate the partial
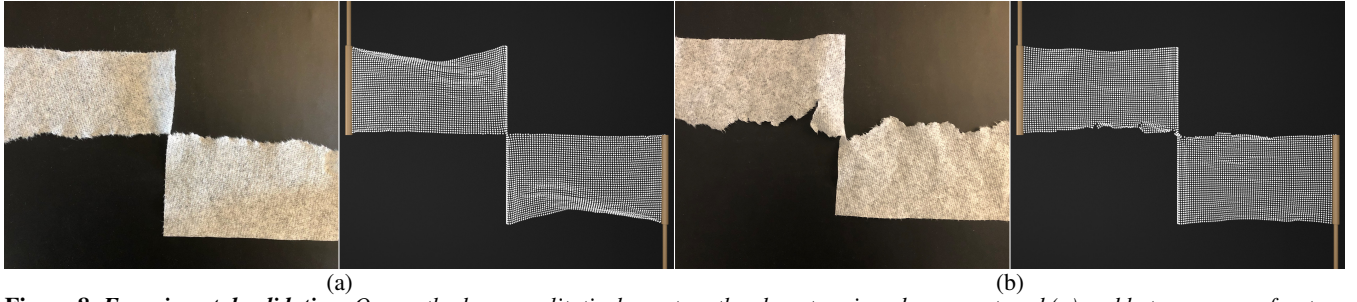
(a)	(b)

Figure 8: *Experimental validation. Our method can qualitatively capture the clean tear in a dry paper towel (a) and heterogeneous fracture in a wet paper towel (b). The real-world images are shown on the left, and simulated images using our formulation are shown on the right.*

Table 1: *We provide a list of the main parameters used in our simulations. E: Young's modulus, μ: Poisson's ratio, ρ: Density, C: Diffusive capacity, k: Coefficient of diffusion, α: Coefficient of linear diffusion expansion, G_f: Material fracture energy, η_0: Elastic deformation thread, Δt: Time step, and Δx: Initial particle distance. All simulations were run on on a 1.80 GHz, Intel(R) Core(TM) i7-8565K CPU with 8GB RAM. The simulation time is measured in average seconds per 20 time steps. Particle: The total number of particles in the simulation.*

Parameters	Large stretching and Shearing	Crack path	Foil	Rubbery Film	Seaweed
E(Pa)	2×10^4	2×10^4	2×10^3	10^2	2×10^4
ν	0.3	0.3	0.3	0.3	0.3
ρ(kg/m^3)	5000	5000	5000	100	100
C (J· K $^{-1}$)	NA	1	1	1	1
k (W/(m·K))	NA	0.01	0.3	1	0.01
α (K^{-1})	NA	1	0.3	10	0.3
G_f	NA	11.3	1.2	11.3	2.4
η_0	NA	10^{-4}	10^{-4}	10^{-3}	10^{-4}
Δt (s)	10^{-4}	10^{-4}	3×10^{-4}	5×10^{-4}	10^{-4}
Δx (m)	0.02	0.02	0.04	0.04	0.04
Particle	10K	10K	2.5K	2.5K	2.5K
Time(s)	0.2	0.2	0.6	0.2	0.2

Figure 9: *XY trajectory of particles. (Left) P1 (0.64, 0.84). (Right) P2 (1.64, 1.64). Our method (black) produces more dynamic motion compared with Smoothed Particle Hydrodynamics (SPH) (red).*

differential equations. Using a PDE-based model, it is challenging to evaluate the derivative along the normal direction as we only use one layer of particles to discretize the sheet. Consequently, those PDE-based methods may not be able to capture the folds in the shearing cases and the wrinkles along the edges of a crack (see Figure 5). In contrast, our proposed integral-based model does not involve the evaluation of differential derivatives, which is essential in PDE-based models which also require the physical field to be sufficiently smooth, and can naturally handle fractures and deformations along the normal direction.

In order to validate our proposed method, we focus on the motion in the XY plane in the large stretching case. We plot the XY trajectory of the particles located at positions P1(0.64, 0.84) and P2(1.64, 1.64) on the sheet obtained using the proposed Lagrangian particle-based formulation and standard Smoothed Particle Hydrodynamics (SPH) [LL03]. Figure 9 shows that our results are close to the results from SPH as the differences occur at a very small order of magnitude, while the trajectory obtained by the proposed method is more dynamic. Our method captures more realistic stretching deformation as shown in Figure 10.
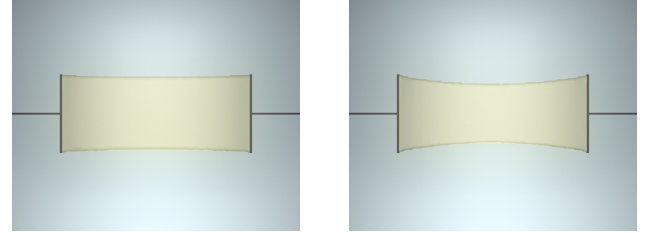

Figure 10: *Comparison between SPH and the proposed method. Our method (right) captures more realistic stretching deformation of an elastic sheet than that obtained by standard SPH (left).*
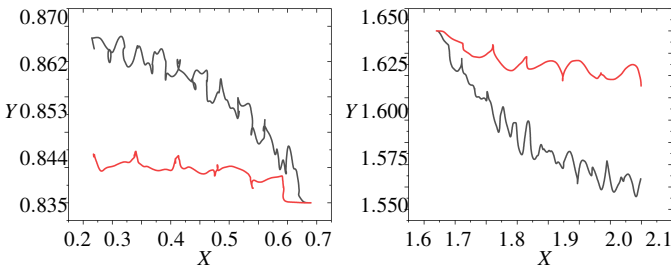
6.2. Crack path

To demonstrate the effects of diffusion evolution on crack branches, we put two sources that diffuse material in a pre-notched thin brittle membrane under tensile loading. Due to the existence of diffusion, extra diffusion-driven stress is introduced to material constitutive laws, leading to the heterogeneously dynamic responses and arbitrary fracture patterns in the membrane. Figure 2 shows that straight cracks grow in the membrane without diffusion, while the crack tip in the membrane with diffusion changes its path and initiates small branches, showcasing a zigzag propagation of the crack. Figure 2(bottom) visualizes the diffusive quantities colored from light red to dark red in the order of increasing values.

6.3. Tearing foil and paper towel

To demonstrate fracture due to out-of-plane motions, we simulated the tearing of aluminum foils with prescribed velocity boundary

conditions on the top edges, as shown in Figure 4. Our Lagrangian particle-based formulation can easily handle the out-of-plane motion while preserving fine details. A "clean" tear was captured in Figure 4 (top) in the absence of diffusion effects. We heated the foil by randomly distributed heat sources on the sheet and simulated the coupling of deformation and heat transfer. In this case, the crack path branches as the temperature changes. Next, as shown in Figure 8, we compared our simulations of tearing dry and wet paper towels with real-world experiments. Our method can qualitatively reproduce straight crack paths of the dry paper towel and irregular crack paths of the wet paper towel, as observed in the real world.

6.4. Rubbery film

Next, we stretch a rubbery film (e.g., a biodegradable film [VBP*20]) using our Lagrangian particle-based formulation with the non-linear elastic constitutive model in equation (19). Figure 5(top) shows how the slit evolves into a dynamic crack as time goes by. At the beginning, the slit has not yet started to grow, wrinkles are visible along the slit edges (see left column in Figure 5). The wrinkles occur because the membrane is free along the edges normal to the slit and, thus, tends to develop compressive strains parallel to the slit. In the remaining views shown in Figure 5, the crack is propagating and wrinkles appear in the wake of the crack. To demonstrate the effects of diffusion, we spray acid solvent on the film. Due to biodegradability, the film begins to dissolve and subsequently leads to heterogeneous fracture patterns, as shown in Figure 5(bottom).

6.5. Seaweed flake

Our method can also be used to simulate realistically brittle membranes, such as seaweed flakes. As shown in Figure 7, a crispy seaweed flake was ripped abruptly. Our Lagrangian particle-based formulation captures vivid brittle fractures displaying symmetric crack patterns, as they grow and branch in a dry seaweed flake (see Figure 7(top)). In contrast, the crack tip in a damp seaweed flake changes its path and exhibits asymmetric crack paths (see Figure 7 (bottom)) due to moisture diffusion.
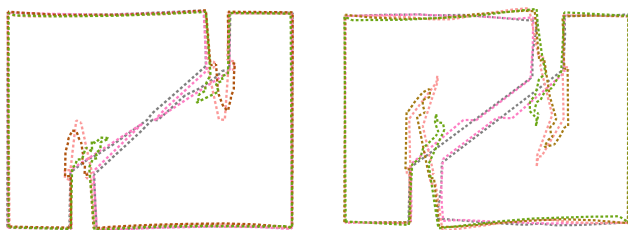

Figure 11: *Effect of long-range force (Non-locality). Grey: R = 0.0681, Light pink: R = 0.0749, Soft red: R = 0.0851, Dark orange R = 0.0953, and Dark green R = 0.102. Our model also shows that long-range forces introduce non-local effects that lead to stiffer material responses, which agree with the observation in [SNRS17].*

6.6. Non-local effect

Our method leads to a non-local model and captures different fracture patterns due to long-range forces. Via tuning the cutoff radius

R in equation (23), the non-local effect is introduced by considering the interaction with more particles in comparison to its local counterpart. We demonstrated that, in the case with long-range forces, the crack grows slower and shows multiple polyline-like patterns, while in cases with less particle interactions, the crack propagates abruptly and demonstrates clean fracture patterns. Our model with large long-range forces gives stiffer material responses, which agree with the observations in 1D for dynamic beam simulation [SNRS17].

7. Discussions and Conclusion

We proposed a Lagrangian particle-based formulation to simulate fractures in thin membrane-like structures. To simulate the heterogeneity in materials that is introduced due to diffusion, we derived a unified framework for coupling together deformation and diffusion. We demonstrated that our method captures realistic fracture propagation in a wide range of materials, such as aluminum foils, rubbery films, and seaweed flakes, and produces more detailed and realistic effects of arbitrary crack branches due to diffusion processes in practical applications.

7.1. Limitations

Our model has generated a large number of compelling examples, but there remains much work to be done. Parameters to adjust the plasticity were tuned by hand, and it would be interesting to calibrate them to measured models. While explicit time integration is a reasonable treatment given that small time steps are required for capturing cracks, it would be interesting to incorporate multi-rate time integration schemes, such as [FHHJ18,GB14], into our framework to support different time steps on different subdomains of the material. Another limitation of our work stems from the particle

Figure 12: *Comparison between particles and mesh. (Left) Surface mesh generated by Houdini [Sid20]. (Right) Raw data of particles. Our raw data of particles provides more realistic details of cracks along the tear and the subtle wrinkles on the membrane surface, which the mesh generated by Houdini fails to capture.*

discretization for crack surface representation. The level of crack detail is highly dependent on the embedded particle resolution. A more detailed crack surface could benefit from a multi-resolution particle discretization, such as [WHK17]. In our stretching simulations (see Figure 3), we also found that our method suffers from area loss as shown by the linear growth in average divergence of the velocity field in Figure 13. As our Lagrangian particle-based formulation is similar to bond-based Peridynamics [GSS05,Sil00], the restriction on Poisson's ratio of 1/4 for plane strain and 1/3 for

plane stress in bond-based Peridynamics also exists in our method, making it unable to enforce incompressibility in a precise fashion. It would be interesting to investigate our method based on *state-based Peridynamics* that can circumvent this restriction on Poisson's ratio. Additionally, meshing with particles also poses a challenge. We used Houdini [Sid20] to generate a surface mesh using our particle data. Although these surfaces can demonstrate the influence of diffusion on the crack path, they fail to extract all information that our simulation provides and may lead to local inversion and numerical noise. This leads to the loss of some subtle details of fractures and wrinkles in the mesh, as shown in Figure 12(left). Our raw data of particles in Figure 12(right), and also in Figure 8, produces realistic wrinkles and crack branches at small scales, while the surface generated by Houdini [Sid20] smooths out these details. Finally, while our focus was on the material responses of an
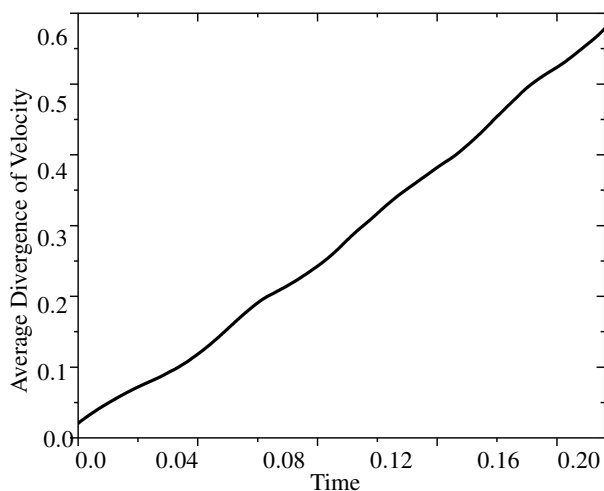

Figure 13: *Velocity divergence for large stretching in Figure 3.*

aluminium foil, a rubbery film, and a crispy seaweed flake, it would be interesting to investigate other material behaviors and diffusion-dependent material properties.

8. Acknowledgements

References

[AD12] APOSTOLAKIS G., DARGUSH G. F.: Mixed lagrangian formulation for linear thermoelastic response of structures. *Journal of engineering mechanics 138*, 5 (2012), 508–518.

[BD10] BOBARU F., DUANGPANYA M.: The peridynamic formulation for transient heat conduction. *International Journal of Heat and Mass Transfer 53*, 19-20 (2010), 4047–4059.

[BDW13] BUSARYEV O., DEY T. K., WANG H.: Adaptive fracture simulation of multi-layered thin plates. *ACM Transactions on Graphics (TOG) 32*, 4 (2013), 1–6.

[BFA02] BRIDSON R., FEDKIW R., ANDERSON J.: Robust treatment of collisions, contact and friction for cloth animation. In *Proceedings of the 29th annual conference on Computer graphics and interactive techniques* (2002), pp. 594–603.

[BILD11] BERGMAN T. L., INCROPERA F. P., LAVINE A. S., DEWITT D. P.: *Introduction to heat transfer*. John Wiley & Sons, 2011.

[BK62] BLATZ P. J., KO W. L.: Application of finite elastic theory to the deformation of rubbery materials. *Transactions of the Society of Rheology 6*, 1 (1962), 223–252.

[CK05] CHOI K.-J., KO H.-S.: Stable but responsive cloth. In *ACM SIGGRAPH 2005 Courses*. 2005, pp. 1–es.

[Cru77] CRUSE T. A.: *Mathematical foundations of the boundary-integral equation method in solid mechanics*. Tech. rep., PRATT AND WHITNEY AIRCRAFT GROUP EAST HARTFORD CONN, 1977.

[CZZ*18] CHEN W., ZHU F., ZHAO J., LI S., WANG G.: Peridynamics-based fracture animation for elastoplastic solids. In *Computer Graphics Forum* (2018), vol. 37, Wiley Online Library, pp. 112–124.

[DCL00] DE CASSON F. B., LAUGIER C.: Simulating 2d tearing phenomena for interactive medical surgery simulators. In *Proceedings Computer Animation 2000* (2000), IEEE, pp. 9–14.

[FHHJ18] FANG Y., HU Y., HU S.-M., JIANG C.: A temporally adaptive material point method with regional time stepping. In *Computer graphics forum* (2018), vol. 37, Wiley Online Library, pp. 195–204.

[GB14] GOSWAMI P., BATTY C.: Regional time stepping for sph. In *Eurographics 2014* (2014), Eurographics Association, pp. 45–48.

[GN06] GUO Y., NAIRN J.: Three-dimensional dynamic fracture analysis using the material point method. *Computer Modeling in Engineering and Sciences 16*, 3 (2006), 141.

[GSH*04] GINGOLD Y., SECORD A., HAN J. Y., GRINSPUN E., ZORIN D.: A discrete model for inelastic deformation of thin shells. In *ACM SIGGRAPH/Eurographics symposium on computer animation* (2004).

[GSS05] GERSTLE W., SAU N., SILLING S.: Peridynamic modeling of plain and reinforced concrete structures.

[Gur82] GURTIN M. E.: *An introduction to continuum mechanics*. Academic press, 1982.

[HHB11] HU W., HA Y. D., BOBARU F.: Modeling dynamic fracture and damage in a fiber-reinforced composite lamina with peridynamics. *International Journal for Multiscale Computational Engineering 9*, 6 (2011).

[HJST13] HEGEMANN J., JIANG C., SCHROEDER C., TERAN J. M.: A level set method for ductile fracture. In *Proceedings of the 12th ACM SIGGRAPH/Eurographics Symposium on Computer Animation* (2013), SCA '13, p. 193–201.

[HWW17] HE X., WANG H., WU E.: Projective peridynamics for modeling versatile elastoplastic materials. *IEEE transactions on visualization and computer graphics 24*, 9 (2017), 2589–2599.

[JGT17] JIANG C., GAST T., TERAN J.: Anisotropic elastoplasticity for cloth, knit and hair frictional contact. *ACM Transactions on Graphics (TOG) 36*, 4 (2017), 1–14.

[KBT17] KOSCHIER D., BENDER J., THUEREY N.: Robust extended finite elements for complex cutting of deformables. *ACM Trans. Graph. 36*, 4 (2017).

[KMB*09] KAUFMANN P., MARTIN S., BOTSCH M., GRINSPUN E., GROSS M.: Enrichment textures for detailed cutting of shells. In *ACM SIGGRAPH 2009 papers*. 2009, pp. 1–10.

[Lad00] LADOPOULOS E.: Non-linear multidimensional singular integral equations in two-dimensional fluid mechanics. *International journal of non-linear mechanics 35*, 4 (2000), 701–708.

[LBC*14] LEVINE J. A., BARGTEIL A. W., CORSI C., TESSENDORF J., GEIST R.: A peridynamic perspective on spring-mass fracture. In *Symposium on Computer Animation* (2014), Citeseer, pp. 47–55.

[LL03]   LIU G.-R., LIU M. B.: *Smoothed particle hydrodynamics: a meshfree particle method*. World scientific, 2003.

[LS67]   LORD H. W., SHULMAN Y.: A generalized dynamical theory of thermoelasticity. *Journal of the Mechanics and Physics of Solids 15*, 5 (1967), 299–309.

[LYO*10]   LEE Y., YOON S.-E., OH S., KIM D., CHOI S.: Multi-resolution cloth simulation. In *Computer Graphics Forum* (2010), vol. 29, Wiley Online Library, pp. 2225–2232.

[LZC*19]   LYU Y., ZHANG J., CHANG J., GUO S., ZHANG J. J.: Integrating peridynamics with material point method for elastoplastic material modeling. In *Computer Graphics International Conference* (2019), Springer, pp. 228–239.

[MBF04]   MOLINO N., BAO Z., FEDKIW R.: A virtual node algorithm for changing mesh topology during simulation. *ACM Transactions on Graphics (TOG) 23*, 3 (2004), 385–392.

[MHHR07]   MÜLLER M., HEIDELBERGER B., HENNIX M., RATCLIFF J.: Position based dynamics. *Journal of Visual Communication and Image Representation 18*, 2 (2007), 109–118.

[MKB*08]   MARTIN S., KAUFMANN P., BOTSCH M., WICKE M., GROSS M.: Polyhedral finite elements using harmonic basis functions. In *Computer Graphics Forum* (2008), vol. 27, Wiley Online Library, pp. 1521–1529.

[MMC16]   MACKLIN M., MÜLLER M., CHENTANEZ N.: Xpbd: position-based simulation of compliant constrained dynamics. In *Proceedings of the 9th International Conference on Motion in Games* (2016), pp. 49–54.

[MST04]   MÜLLER M., SCHIRM S., TESCHNER M.: Interactive blood simulation for virtual surgery based on smoothed particle hydrodynamics. *Technology and Health Care 12*, 1 (2004), 25–31.

[Mül08]   MÜLLER M.: Hierarchical position based dynamics.

[Nai03]   NAIRN J. A.: Material point method calculations with explicit cracks. *Computer Modeling in Engineering and Sciences 4*, 6 (2003), 649–664.

[NMK*06]   NEALEN A., MÜLLER M., KEISER R., BOXERMAN E., CARLSON M.: Physically based deformable models in computer graphics. In *Computer graphics forum* (2006), vol. 25, Wiley Online Library, pp. 809–836.

[NTB*91]   NORTON A., TURK G., BACON B., GERTH J., SWEENEY P.: Animation of fracture by physical modeling. *The visual computer 7*, 4 (1991), 210–219.

[OBH02]   O'BRIEN J. F., BARGTEIL A. W., HODGINS J. K.: Graphical modeling and animation of ductile fracture. In *Proceedings of the 29th annual conference on Computer graphics and interactive techniques* (2002), pp. 291–294.

[Ogd72]   OGDEN R. W.: Large deformation isotropic elasticity–on the correlation of theory and experiment for incompressible rubberlike solids. *Proceedings of the Royal Society of London. A. Mathematical and Physical Sciences 326*, 1567 (1972), 565–584.

[OH99]   O'BRIEN J. F., HODGINS J. K.: Graphical modeling and animation of brittle fracture. In *Proceedings of the 26th annual conference on Computer graphics and interactive techniques* (1999), pp. 137–146.

[P*95]   PROVOT X., ET AL.: Deformation constraints in a mass-spring model to describe rigid cloth behaviour. In *Graphics interface* (1995), Canadian Information Processing Society, pp. 147–147.

[PGBT18]   PEER A., GISSLER C., BAND S., TESCHNER M.: An implicit sph formulation for incompressible linearly elastic solids. In *Computer Graphics Forum* (2018), vol. 37, Wiley Online Library, pp. 135–148.

[PKA*05]   PAULY M., KEISER R., ADAMS B., DUTRÉ P., GROSS M., GUIBAS L. J.: Meshless animation of fracturing solids. *ACM Transactions on Graphics (TOG) 24*, 3 (2005), 957–964.

[PNDJO14]   PFAFF T., NARAIN R., DE JOYA J. M., O'BRIEN J. F.: Adaptive tearing and cracking of thin sheets. *ACM Transactions on Graphics (TOG) 33*, 4 (2014), 1–9.

[SA05]   SILLING S. A., ASKARI E.: A meshfree method based on the peridynamic model of solid mechanics. *Computers & structures 83*, 17-18 (2005), 1526–1535.

[SB05]   SILLING S. A., BOBARU F.: Peridynamic modeling of membranes and fibers. *International Journal of Non-Linear Mechanics 40*, 2-3 (2005), 395–409.

[SB12]   SIFAKIS E., BARBIC J.: Fem simulation of 3d deformable solids: A practitioner's guide to theory, discretization and model reduction. In *ACM SIGGRAPH 2012 Courses* (2012).

[SDF07]   SIFAKIS E., DER K. G., FEDKIW R.: Arbitrary cutting of deformable tetrahedralized objects. In *Proceedings of the 2007 ACM SIGGRAPH/Eurographics symposium on Computer animation* (2007), pp. 73–80.

[Sid20]   SIDEFX: Houdini, 2020.

[Sil00]   SILLING S. A.: Reformulation of elasticity theory for discontinuities and long-range forces. *Journal of the Mechanics and Physics of Solids 48*, 1 (2000), 175–209.

[SL10]   SILLING S. A., LEHOUCQ R. B.: Peridynamic theory of solid mechanics. *Advances in applied mechanics 44* (2010), 73–168.

[SNRS17]   SARKAR S., NOWRUZPOUR M., REDDY J., SRINIVASA A.: A discrete lagrangian based direct approach to macroscopic modelling. *Journal of the Mechanics and Physics of Solids 98* (2017), 172–180.

[SOG06]   STEINEMANN D., OTADUY M. A., GROSS M.: Fast arbitrary splitting of deforming objects. In *Proceedings of the 2006 ACM SIGGRAPH/Eurographics symposium on Computer animation* (2006), pp. 63–72.

[SRH17]   SCHRECK C., ROHMER D., HAHMANN S.: Interactive paper tearing. In *Computer Graphics Forum* (2017), vol. 36, Wiley Online Library, pp. 95–106.

[TF88]   TERZOPOULOS D., FLEISCHER K.: Modeling inelastic deformation: viscolelasticity, plasticity, fracture. In *Proceedings of the 15th annual conference on Computer graphics and interactive techniques* (1988), pp. 269–278.

[Tre44]   TRELOAR L.: Stress-strain data for vulcanized rubber under various types of deformation. *Rubber Chemistry and Technology 17*, 4 (1944), 813–825.

[VBP*20]   VIVCHARENKO V., BENKO A., PALKA K., WOJCIK M., PRZEKORA A.: Elastic and biodegradable chitosan/agarose film revealing slightly acidic ph for potential applications in regenerative medicine as artificial skin graft. *International Journal of Biological Macromolecules 164* (2020), 172–183.

[WCL*20]   WOLPER J., CHEN Y., LI M., FANG Y., QU Z., LU J., CHENG M., JIANG C.: Anisompm: Animating anisotropic damage mechanics. *ACM Trans. Graph. 39*, 4 (2020).

[WDG*19]   WANG S., DING M., GAST T. F., ZHU L., GAGNIERE S., JIANG C., TERAN J. M.: Simulation and visualization of ductile fracture with the material point method. *Proc. ACM Comput. Graph. Interact. Tech. 2*, 2 (2019).

[WFL*19]   WOLPER J., FANG Y., LI M., LU J., GAO M., JIANG C.: Cdmpm: continuum damage material point methods for dynamic fracture animation. *ACM Transactions on Graphics (TOG) 38*, 4 (2019), 1–15.

[WHK17]   WINCHENBACH R., HOCHSTETTER H., KOLB A.: Infinite continuous adaptivity for incompressible sph. *ACM Transactions on Graphics (TOG) 36*, 4 (2017), 1–10.

[WSG05]   WICKE M., STEINEMANN D., GROSS M.: Efficient animation of point-sampled thin shells. In *Computer Graphics Forum* (2005), vol. 24, Citeseer, pp. 667–676.

[XSH*20]   XUE T., SU H., HAN C., JIANG C., AANJANEYA M.: A novel discretization and numerical solver for non-fourier diffusion. *ACM Transactions on Graphics (TOG) 39*, 6 (2020), 1–14.

[XZT19]   XUE T., ZHANG X., TAMMA K. K.: A non-local dissipative lagrangian modelling for generalized thermoelasticity in solids. *Applied Mathematical Modelling 73* (2019), 247–265.

[ZTNZ77] ZIENKIEWICZ O. C., TAYLOR R. L., NITHIARASU P., ZHU J.: *The finite element method*, vol. 3. McGraw-hill London, 1977.

[ZTTT00] ZIENKIEWICZ O. C., TAYLOR R. L., TAYLOR R. L., TAYLOR R. L.: *The finite element method: solid mechanics*, vol. 2. Butterworth-heinemann, 2000.

Appendix A: Comparison with classical elastic material

Consider homogeneous deformation as $\mathbf{F} = \mathbf{I} + \nabla \mathbf{u}$ for membrane-like structures, where $\mathbf{u}$ denotes the displacement and assume that in some Cartesian coordinate system the components of $\mathbf{F}$ are given by:

$$\mathbf{F} = \begin{bmatrix} \lambda_1 & 0 \\ 0 & \lambda_2 \end{bmatrix} \qquad (29)$$

where λ_1 and λ_2 are the principal stretches, and the out-of-plane stretch is ignored as the out-of-plane stress component vanishes in membrane-like structures. The bulk response of particle i will be determined by finding the strain energy $\Psi(\mathbf{F})$ per unit volume contained in all the micro-bonds connected to particle i in the body. Now we can rewrite the bond stretch in equation (10) based on equation (29),

$$s_{ij} = \frac{\|\mathbf{r}_{ij}\|}{\|\mathbf{r}_{ij}^0\|} = \sqrt{\lambda_1^2 \cos^2 \theta + \lambda_2^2 \sin^2 \theta} \qquad (30)$$

Based on the strain energy in [Sil00], we have the following integration form of the strain energy:

$$\Psi(\mathbf{F}) = \frac{h}{2} \int_0^\delta \int_0^{2\pi} \phi(s(\theta, r)) r d\theta dr = \frac{\pi h c R}{2} \left(\lambda_1^2 + \lambda_2^2 + \frac{2}{\lambda_1 \lambda_2} - 4 \right) \qquad (31)$$

where $\phi(s(\theta, r))$ represents the strain energy of a micro-bond and the influence radius R can be defined as follows:

$$R = \int_0^\delta r W(r) dr \qquad (32)$$

where $W(r)$ denotes the weighted function in equation (23). The macroscopic strain energy density $\Psi(\mathbf{F})$ in equation (31) depends only on the two principle stretches and does not explicitly include any out-of-plane stretch. However, this $\Psi(\mathbf{F})$ can be further expressed as follows:

$$\Psi(\mathbf{F}) = \frac{\pi h c R}{2} \left(\lambda_1^2 + \lambda_2^2 + \lambda_3^2 + \frac{1}{\lambda_1 \lambda_2 \lambda_3} - 4 \right) \qquad (33)$$

where λ_3 represents the out-of-plane stretch. The material specified in equation (33) is a special case for the Blatz-Ko materials, which has been widely used to describe materials like rubber [BK62, Ogd72, Tre44].